Synthesis, Shape Control, and Methanol Electro-oxidation Properties of Pt–Zn Alloy and Pt_3Zn Intermetallic Nanocrystals

Yijin Kang,[†] Jun Beom Pyo,[‡] Xingchen Ye,[†] Thomas R. Gordon,[†] and Christopher B. Murray[†,‡,*]

[†]Department of Chemistry and [‡]Department of Materials Science and Engineering, University of Pennsylvania, Philadelphia, Pennsylvania 19104, United States

ABSTRACT

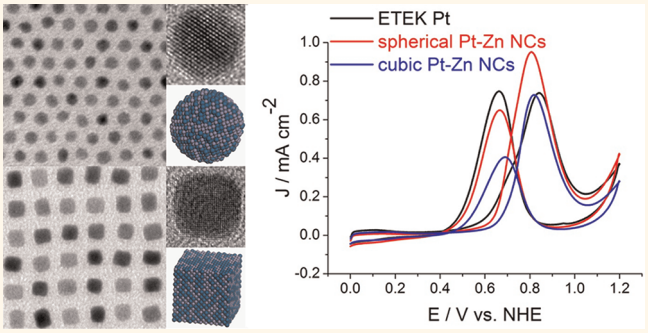

We report the first synthesis of highly monodisperse Pt_3Zn nanocrystals (NCs). Shape-controlled synthesis generates cubic and spherical Pt–Zn NCs. Reaction temperature is the key to incorporate Zn into Pt, even in the absence of a strong reducing agent. The Pt–Zn NCs are active toward methanol oxidation, with the spherical NCs exhibiting higher activity than the cubic NCs. The Pt–Zn alloy phase can be transformed into the Pt_3Zn intermetallic phase, upon annealing. The intermetallic Pt_3Zn shows better performance than the alloy phase Pt–Zn. Besides the activity toward methanol oxidation, Pt–Zn NCs show excellent poisoning tolerance. With activities comparable to the commercial Pt catalyst, enhanced poisoning tolerance and lower cost, Pt–Zn and Pt_3Zn NCs are a promising new family of catalysts for direct methanol fuel cells.

KEYWORDS: platinum · zinc · electrocatalysis · methanol oxidation · intermetallic · shape control · nanocrystal

Polymer electrolyte membrane fuel cells (PEMFCs) have been intensively studied, particularly for the powering of portable devices.[1,2] Due to issues with the handling of hydrogen, direct use of liquid fuels such as small organic molecules has been receiving great attention.[2] Pt is the best catalyst of all pure metals for the oxidation of small organic molecules; however, its high cost and low CO poisoning tolerance severely limit the wider adoption of Pt catalysts.[3] Tremendous efforts have been made to improve the activity and poisoning tolerance of electrocatalysts, as well as to reduce the cost.[2] One direction to achieve these goals is to control the morphology (shape) of catalysts,[4–10] while another important direction is the preparation of Pt-based alloys or intermetallic compounds[2,6,11–22] to reduce the overall Pt loading for a desired performance level. For instance, Pt–Ru,[23,24] Mn–Pt,[25] Cu–Pt,[26] Pt_3Sc,[27] Pt_3Y,[27] Pt_3Ni,[15,22] PtPb,[11,13,28] PtBi,[11,13] and PtZn[29] have been reported as promising candidates of fuel cell catalysts.

Recently, intermetallic PtZn particles with high activities toward formic acid and methanol oxidation have been prepared by reaction of Pt in Zn vapor.[29] However, to our knowledge, the direct synthesis of Pt–Zn nanocrystals (NCs) has not been achieved. In this work, we report the first synthesis and shape control of Pt–Zn alloy and Pt_3Zn intermetallic NCs. Compared to the commercial Pt catalyst, Pt–Zn NCs show superior poisoning tolerance for methanol oxidation while maintaining comparable activities.

RESULTS AND DISCUSSION

For the synthesis of spherical Pt–Zn NCs, platinum acetylacetonate [$Pt(acac)_2$] and zinc acetylacetonate [$Zn(acac)_2$] are dissolved in oleylamine and oleic acid, which are used as both stabilizers and solvents. Then, the well mixed solution is brought to 350 °C at the heating rate of 30 °C/min and is kept at this temperature for 30–60 min. Cubic Pt–Zn NCs (Figure 1a,b and Figure S1 in Supporting Information) are made by adding benzyl ether, while spherical Pt–Zn NCs (Figure 1c,d) are produced in the absence of benzyl ether. The yield of Pt–Zn NCs is ~100% (Pt basis). From transmission

* Address correspondence to cbmurray@sas.upenn.edu.

Received for review April 10, 2012 and accepted May 4, 2012.

Published online May 04, 2012
10.1021/nn301583g

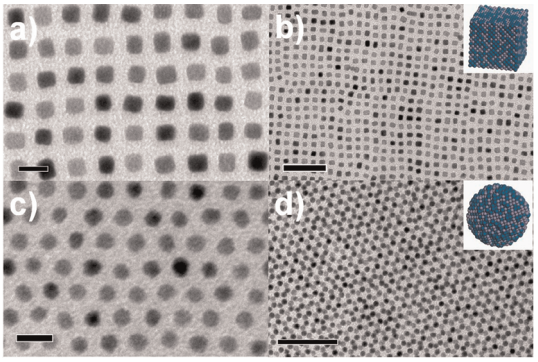

Figure 1. TEM images of (a,b) cubic Pt−Zn NCs and (c,d) spherical Pt−Zn NCs. Insets in b and d are graphic models of Pt−Zn cubic NCs and spherical NCs. The gray and blue balls represent Zn and Pt atoms, respectively. Scale bars: (a,c) 10 nm and (b,d) 50 nm.

electron microscope (TEM) images shown in Figure 1, the size of Pt−Zn NCs is measured to be 4.5 nm (diameter, σ < 5%) for spherical NCs and 6.9 nm (edge length, σ = 8%) for cubic NCs. The high-resolution TEM (HRTEM) images (Figure 2) indicate that both spherical and cubic Pt−Zn NCs are single crystals with high crystallinity. The HRTEM images also reveal an interplanar distance of about 0.19 nm for a cubic Pt−Zn NC (corresponding to the lattice spacing of the Pt_3Zn {200} planes) and interplanar distances of about 0.27 and 0.22 nm for a spherical Pt−Zn NC (corresponding to the lattice spacing of the Pt_3Zn {110} and {111} planes, respectively). The selected area electron diffraction (SAED) pattern (Figure S1) of the cubic Pt−Zn NCs confirms the high crystallinity and indicates the (100) texture of the cubic Pt−Zn NCs by an enhanced {200} diffraction. The as-synthesized NCs are actually Pt−Zn alloys at a stoichiometry of Pt/Zn = 3:1, which is determined by both energy-dispersive X-ray spectra (EDX) and inductively coupled plasma optical emission spectrometry (ICP-OES). After annealing at 600 °C for 30 min, the alloy phase is converted to the ordered intermetallic phase ($AuCu_3$ structure, JCPDS 65-3257; Figure 3 and Figure S2).

Among many reaction parameters, the temperature of synthesis is the most important in dictating the Pt/Zn ratio. As shown in Figure 4a, syntheses carried out in the range of 300−330 °C produce Pt−Zn alloys with less than 25% (mol) Zn, and below 270 °C, pure Pt NCs are produced. The composition of final alloy products is independent of the Pt/Zn ratio in the reaction precursors, as examples (syntheses carried out at 300 °C) shown in Figure 4b. A control experiment is performed by decomposing $Zn(acac)_2$ in oleic acid and oleylamine (*i.e.*, in the absence of Pt). This reaction generates wurtzite phase ZnO NCs, as shown in Figure S4. In contrast, in the synthesis of Pt−Zn alloy NCs (*i.e.*, in the presence of Pt), the ZnO is never observed. Apparently, the high reaction temperature is the key to incorporate Zn into Pt, even in the absence of a strong reducing

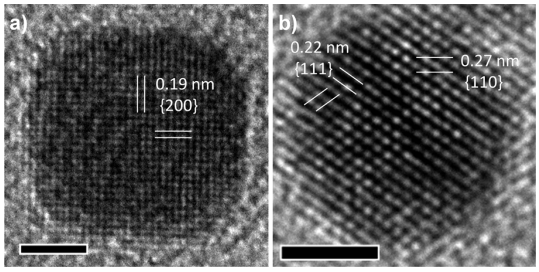

Figure 2. HRTEM images of (a) cubic Pt−Zn NCs and (b) spherical Pt−Zn NCs. Scale bars: 2 nm.

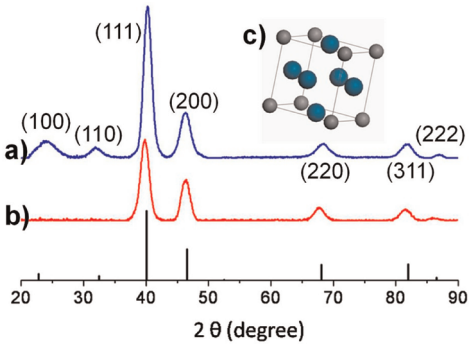

Figure 3. XRD patterns of (a) intermetallic phase Pt_3Zn NCs after annealing of as-synthesized cubic Pt−Zn NCs at 600 °C and (b) as-synthesized cubic Pt−Zn NCs; (c) unit cell of Pt_3Zn. The gray and blue balls represent Zn and Pt atoms, respectively.

agent. We have also demonstrated in a previous report that using a high reaction temperature is an effective way to dope the nanophosphors with rare earth elements.[30] What reduces Zn^{2+} to Zn^0 remains unclear so far. Nevertheless, that high reaction temperature can facilitate the formation of alloy or doped NCs is well demonstrated.

The combination of oleic acid and oleylamine as capping agent is essential to the synthesis of monodisperse Pt−Zn NCs. The ultrasmall NCs with an irregular shape are produced in the absence of oleylamine (Figure S5a), and NCs with broad size distribution are produced in the absence of oleic acid (Figure S5b). The presence of oleylamine and benzyl ether appears to be the key to obtain cubic Pt−Zn NCs. No cubic NCs are found using oleic acid and benzyl ether as ligand and solvent (Figure S5c), while a mixture of both spherical and cubic NCs is observed when oleylamine and benzyl ether are used (Figure S5d). Notably, using other high boiling point solvents, such as diphenyl ether (DPE) or 1-octadecene (ODE), also produces spherical NCs (Figure S6).

The methanol electro-oxidation properties of the Pt−Zn NCs are tested in 0.5 M methanol + 0.1 M H_2SO_4 solution. As shown in Figure 5a, the Pt−Zn NCs have comparable maximum methanol electro-oxidation activity (current density normalized to catalyst surface area) to commercial ETEK Pt catalyst. The typical

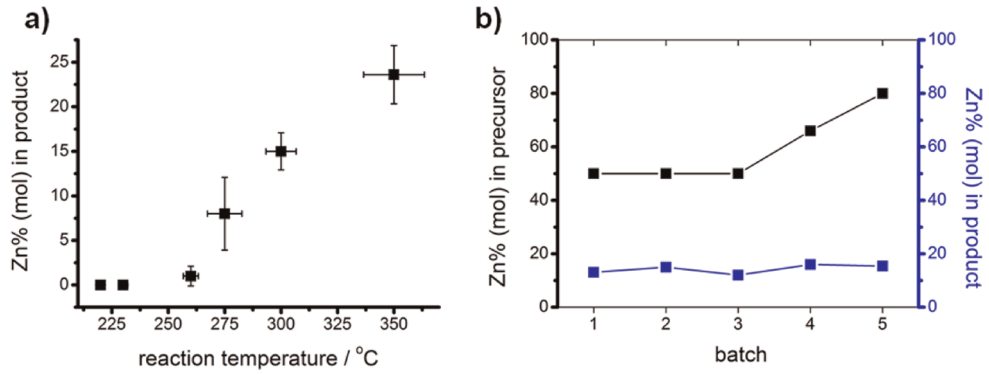

Figure 4. Zn ratio in the product of Pt−Zn NCs is (a) dependent on reaction temperature of syntheses and (b) independent of the Zn ratio in the precursor (reactions at 300 °C).

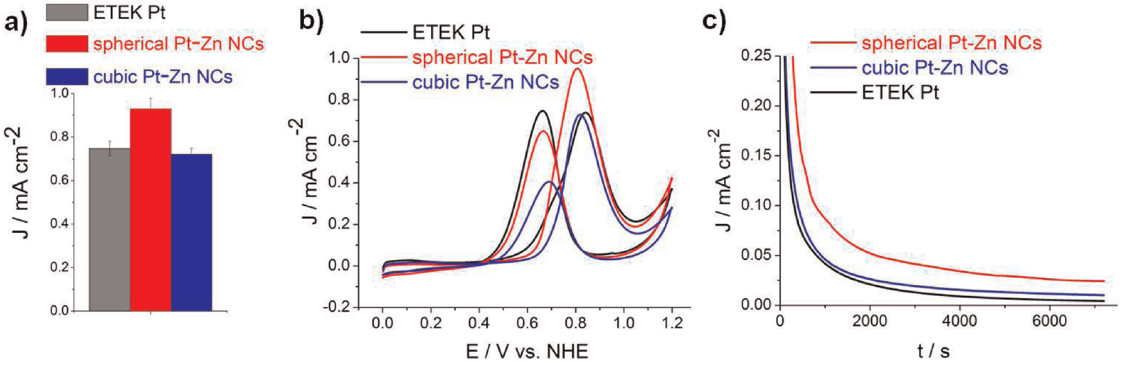

Figure 5. (a) Surface area normalized activities and (b) representative polarization curves of methanol oxidation on spherical Pt−Zn NCs, cubic Pt−Zn NCs, and ETEK Pt; (c) chronoamperometric curves of methanol oxidation on spherical Pt−Zn NCs, cubic Pt−Zn NCs, and ETEK Pt at 0.8 V. All measurements are carried out in 0.5 M methanol + 0.1 M H_2SO_4.

methanol oxidation polarization curves for spherical Pt−Zn NCs, cubic Pt−Zn NCs, and ETEK Pt are shown in Figure 5b. The current density peak in the forward sweep is ascribed to the methanol oxidation on the catalyst, which forms CO, CO_2, and other carbonaceous intermediates that adsorb onto the catalyst surface. During the backward sweep, the adsorbed carbonaceous species are further oxidized to CO_2, which contributes to the current density peak around 0.65 V. Therefore, the ratio of forward sweep current density peak to backward sweep peak, J_f/J_b, can be used to describe the tolerance of catalyst to the carbonaceous species accumulation. In Figure 5b, the ratio of J_f/J_b is 1.46 and 1.80 for spherical and cubic Pt−Zn NCs, respectively, much higher than 0.99 for ETEK Pt. In contrast to previous studies of Pt and Pt alloys in which cubic NCs (or {100} facets) show higher activity than spheres (or mixture of {100} and {111} facets) in H_2SO_4,[25,26,31] here spherical Pt−Zn NCs are shown to exhibit better methanol oxidation activity than cubic NCs in both H_2SO_4 and $HClO_4$ (Figure S8), suggesting that the sulfate anion adsorption effect may be very weak on the Pt−Zn surface.[25,31] The chronoamperometric measurements further confirm that the methanol oxidation activity on spherical Pt−Zn NCs is higher than that on cubic Pt−Zn NCs (Figure 5c).

In the methanol oxidation reactions performed on a rotating disk electrode (RDE), a current density drop from three successive measurements after the current density reached the maximum on ETEK Pt catalysts is observed (Figure 6a). This current density drop is ascribed to the poisoning of the catalyst at an accelerated rate due to the fact that the RDE brings the reactant to the electrode much faster than the pure diffusion. However, this accelerated poisoning effect is not observed on spherical Pt−Zn NCs supported on carbon, on which the polarization curves of three successive measurements are nearly identical (Figure 6b). The current drop is found neither on cubic Pt−Zn NCs nor on spherical Pt−Zn NCs (Figure S9), implying that Pt−Zn has higher poisoning tolerance than pure Pt.

The methanol oxidation activities for the alloy phase Pt−Zn and intermetallic phase Pt_3Zn are also compared. High temperature annealing (600 °C, 30 min) is necessary to obtain the intermetallic Pt_3Zn phase. Considering that the morphology of cubic NCs changes under such high temperature, the spherical Pt−Zn NCs are used to make this comparison. The alloy phase Pt−Zn/C catalysts are made by loading as-synthesized spherical Pt−Zn NCs onto Vulcan XC72R (Cabot), followed by a thermal treatment under air at

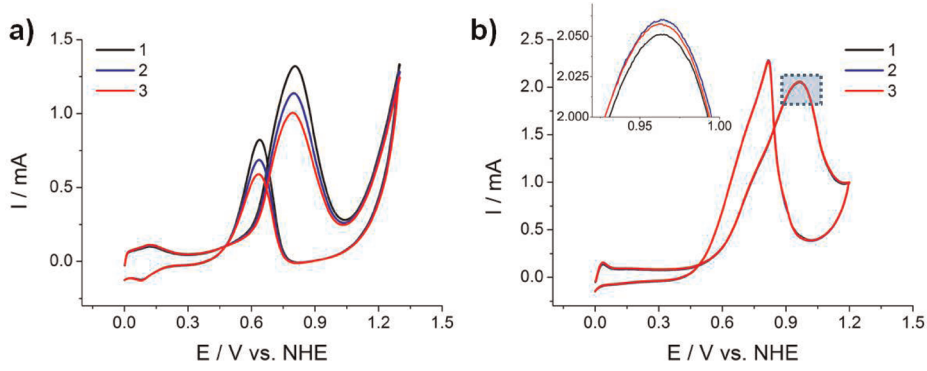

Figure 6. Polarization curves of three successive RDE measurements taken on (a) ETEK Pt and (b) Pt−Zn/C, after the maximum methanol oxidation current densities were reached. Inset of (b): magnified view of selected area in (b). All measurements are carried out in 0.5 M methanol + 0.1 M H_2SO_4 at a rotating rate of 2500 rpm.

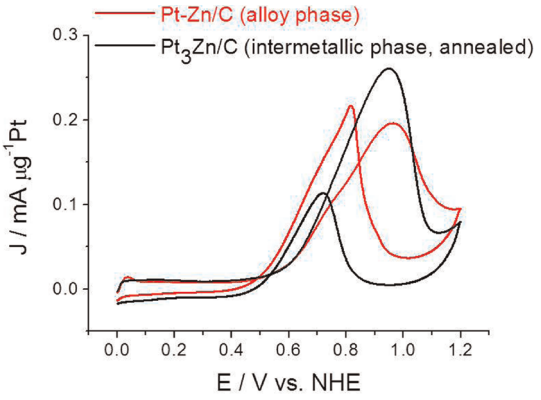

Figure 7. Polarization curves of methanol oxidation on alloy phase Pt−Zn/C and intermetallic phase Pt_3Zn/C catalysts.

210 °C to remove the organic ligands (Figure S10a,b). The intermetallic Pt_3Zn catalysts are prepared by annealing the alloy phase Pt−Zn catalysts at 600 °C for 30 min (Figure S10c,d). As shown on Figure 7, the activities on two catalysts are similar, while the intermetallic phase Pt_3Zn has a higher J_f/J_b ratio than the alloy phase Pt−Zn, implying that the intermetallic phase has greater tolerance to carbonaceous poisoning than the alloy phase of Pt−Zn. Considering the surface area loss of the NCs as a result of sintering and coalescence at high temperature, the intermetallic Pt_3Zn could potentially have even higher activity, if optimized. Other minor factors may also contribute to the enhaced performance. For instance, the high temperature treatment may slightly change the surface composition and structure of Pt−Zn catalysts. Leaching of Zn is possible, although it usually occurs when the concentration of labile element (here, Zn) is equal to or higher than that of noble element (here, Pt).[32] Nevertheless, a high temperature annealing further improves the electrocatalytic performance of Pt−Zn nanocrystals.

CONCLUSION

In summary, we have synthesized highly monodisperse cubic and spherical Pt−Zn NCs and the intermetallic Pt_3Zn/C catalyst. The Pt−Zn and Pt_3Zn NCs are active toward methanol oxidation, with the spherical NCs exhibiting higher activity than the cubic NCs. The Pt−Zn alloy phase can be transformed into the Pt_3Zn intermetallic phase, upon annealing. The intermetallic Pt_3Zn shows better performance than the alloy phase Pt−Zn. Although the Pt−Zn NCs show lower activity toward methanol oxidation than Pt−Mn,[25] Pt−Co,[33] and Pt−Cu,[26] the Pt−Zn NCs are greatly advantageous in terms of excellent poisoning tolerance and low cost of Zn. With activities comparable to commercial Pt catalyst, enhanced poisoning tolerance and lower cost, Pt−Zn and Pt_3Zn NCs are a promising new family of catalysts for direct methanol fuel cells.

METHODS

Synthesis of Spherical Pt−Zn NCs. First, 0.08 g of $Pt(acac)_2$ and 0.05 g (anhydrous basis) of $Zn(acac)_2$ are dissolved in 15 mL of oleylamine and 2.5 mL of oleic acid under N_2 atmosphere. The solution is brought to 350 °C and is kept at this temperature for 30−60 min. The reaction mixture is cooled and purified by hexane/ethanol. The final products are redispersed in hexane.

Synthesis of Cubic Pt−Zn NCs. First, 0.08 g of $Pt(acac)_2$ and 0.05 g (anhydrous basis) of $Zn(acac)_2$ are dissolved in 7.5 mL of oleylamine, 1.25 mL of oleic acid, and 5 mL of benzyl ether under N_2 atmosphere. The solution is brought to 330 °C and is kept at this temperature for 30−60 min (Caution: strong heating power may cause danger). The reaction mixture is cooled and purified by hexane/ethanol. The final products are redispersed in hexane.

Characterization. TEM images are taken on JEOL1400 TEM at 120 kV. The HRTEM image and energy-dispersive X-ray spectroscopy (EDX) are taken on JEOL2010F TEM at 200 kV. X-ray diffraction (XRD) patterns are obtained on a Rigaku smartlab diffractometer with Cu Kα radiation (λ = 1.5418 Å). Quantitative elemental analyses for the composition of catalysts are carried out with both EDX and ICP-OES on a SPECTRO GENESIS ICP spectrometer.

Electrochemical Measurements. Electrochemical measurements are performed on a potentiostat (Epsilon, Bioanalytical Systems Inc.) equipped with a rotating disk electrode (RDE). Ag/AgCl electrode is used as reference electrode, and a platinum coil is used as counter electrode. All potentials are converted to values with reference to a normal hydrogen electrode (NHE). The electrolyte is 0.1 M sulfuric acid if not specified. All water used in experiments is Millipore ultrapure water (18.2 MΩ).

Preparation of Working Electrode. For commercial Pt/C catalyst (20 wt % Pt, ETEK), an aqueous dispersion (1.5 mg/mL) is prepared and sonicated for 60 min. Twenty microliters of the dispersion is then transferred onto the glassy carbon RDE with a 6 mm diameter. For Pt−Zn NC catalysts, the sample is adjusted to ~1 mg Pt/mL (based on ICP-OES measurement) and 5 μL of the solution (in hexane) is transferred onto the RDE. The actual loadings are determined by ICP-OES. Pt−Zn NC thin film catalysts are treated by UV/ozone for 10 h to remove organic capping agents before measurements.

Measurement of Catalyst Surface Area. The catalyst surface area is determined electrochemically by adsorption−desorption of hydrogen between 0.05 and 0.4 V and assuming 210 μC/cm^2 for a monolayer of adsorbed hydrogen on the Pt surface. All cyclic voltammetry (CV) measurements are carried out at room temperature under a flow of nitrogen gas at a sweep rate of 100 mV/s.

Measurement of Methanol Oxidation Reaction. All measurements are carried out at room temperature in 0.1 M H_2SO_4 (or $HClO_4$) + 0.5 M methanol at a sweep rate of 20 mV/s. The sweeps at maximum current densities are recorded. Usually, the maximum current density is obtained in the first or second sweep on ETEK Pt and in the second or third sweep on Pt−Zn NCs. The RDE (2500 rpm) is used in the poisoning tolerance studies.

Conflict of Interest: The authors declare no competing financial interest.

Acknowledgment. Y.J.K. acknowledges partial support from the U.S. Army Research Office (ARO) under award number MURI W911NF-08-1-0364. J.P. acknowledges the support by the Rachleff Scholars Program. X.Y. is supported by the Office of Naval Research (ONR) Multidisciplinary University Research Initiative (MURI) on Optical Metamaterials through award N00014-10-1-0942, while T.R.G. is supported by the Nano/Bio Interface Center through the National Science Foundation NSEC under award number DMR08-32802. C.B.M. is grateful to Richard Perry professorship and the support by the National Science Foundation though PENN MRSEC DMR-0520020. We thank Douglas Yates at the Penn Regional Nanotechnology Facility for support in electron microscopy, and David Vann at Department of Earth and Environmental Science (University of Pennsylvania) for support in ICP-OES.

Supporting Information Available: Additional figures. This material is available free of charge *via* the Internet at http://pubs.acs.org.

REFERENCES AND NOTES

1. Steele, B. C. H.; Heinzel, A. Materials for Fuel-Cell Technologies. *Nature* **2001**, *414*, 345–352.
2. Gasteiger, H. A.; Kocha, S. S.; Sompalli, B.; Wagner, F. T. Activity Benchmarks and Requirements for Pt, Pt-Alloy, and Non-Pt Oxygen Reduction Catalysts for PEMFCs. *Appl. Catal., B* **2005**, *56*, 9–35.
3. Ferreira, P. J.; La'O, G. J.; Shao-Horn, Y.; Morgan, D.; Makharia, R.; Kocha, S.; Gasteiger, H. A. Instability of Pt/C Electrocatalysts in Proton Exchange Membrane Fuel Cells - A Mechanistic Investigation. *J. Electrochem. Soc.* **2005**, *152*, A2256–A2271.
4. Narayanan, R.; El-Sayed, M. A. Shape-Dependent Catalytic Activity of Platinum Nanoparticles in Colloidal Solution. *Nano Lett.* **2004**, *4*, 1343–1348.
5. Habas, S. E.; Lee, H.; Radmilovic, V.; Somorjai, G. A.; Yang, P. Shaping Binary Metal Nanocrystals through Epitaxial Seeded Growth. *Nat. Mater.* **2007**, *6*, 692–697.
6. Lim, B.; Jiang, M. J.; Camargo, P. H. C.; Cho, E. C.; Tao, J.; Lu, X. M.; Zhu, Y. M.; Xia, Y. A. Pd−Pt Bimetallic Nanodendrites with High Activity for Oxygen Reduction. *Science* **2009**, *324*, 1302–1305.
7. Kang, Y. J.; Ye, X. C.; Murray, C. B. Size- and Shape-Selective Synthesis of Metal Nanocrystals and Nanowires Using CO as a Reducing Agent. *Angew. Chem., Int. Ed.* **2010**, *49*, 6156–6159.
8. Wang, C.; Daimon, H.; Onodera, T.; Koda, T.; Sun, S. H. A General Approach to the Size- and Shape-Controlled Synthesis of Platinum Nanoparticles and Their Catalytic Reduction of Oxygen. *Angew. Chem., Int. Ed.* **2008**, *47*, 3588–3591.
9. Wang, C.; Daimon, H.; Sun, S. H. Dumbbell-like Pt-Fe_3O_4 Nanoparticles and Their Enhanced Catalysis for Oxygen Reduction Reaction. *Nano Lett.* **2009**, *9*, 1493–1496.
10. Wang, D. Y.; Kang, Y. J.; Doan-Nguyen, V.; Chen, J.; Kungas, R.; Wieder, N. L.; Bakhmutsky, K.; Gorte, R. J.; Murray, C. B. Synthesis and Oxygen Storage Capacity of Two-Dimensional Ceria Nanocrystals. *Angew. Chem., Int. Ed.* **2011**, *50*, 4378–4381.
11. Casado-Rivera, E.; Volpe, D. J.; Alden, L.; Lind, C.; Downie, C.; Vazquez-Alvarez, T.; Angelo, A. C. D.; DiSalvo, F. J.; Abruna, H. D. Electrocatalytic Activity of Ordered Intermetallic Phases for Fuel Cell Applications. *J. Am. Chem. Soc.* **2004**, *126*, 4043–4049.
12. Zhang, J. L.; Vukmirovic, M. B.; Xu, Y.; Mavrikakis, M.; Adzic, R. R. Controlling the Catalytic Activity of Platinum-Monolayer Electrocatalysts for Oxygen Reduction with Different Substrates. *Angew. Chem., Int. Ed.* **2005**, *44*, 2132–2135.
13. Roychowdhury, C.; Matsumoto, F.; Zeldovich, V. B.; Warren, S. C.; Mutolo, P. F.; Ballesteros, M.; Wiesner, U.; Abruna, H. D.; DiSalvo, F. J. Synthesis, Characterization, and Electrocatalytic Activity of PtBi and PtPb Nanoparticles Prepared by Borohydride Reduction in Methanol. *Chem. Mater.* **2006**, *18*, 3365–3372.
14. Stamenkovic, V. R.; Mun, B. S.; Mayrhofer, K. J. J.; Ross, P. N.; Markovic, N. M. Effect of Surface Composition on Electronic Structure, Stability, and Electrocatalytic Properties of Pt-Transition Metal Alloys: Pt-Skin *versus* Pt-Skeleton Surfaces. *J. Am. Chem. Soc.* **2006**, *128*, 8813–8819.
15. Stamenkovic, V. R.; Fowler, B.; Mun, B. S.; Wang, G. F.; Ross, P. N.; Lucas, C. A.; Markovic, N. M. Improved Oxygen Reduction Activity on $Pt_3Ni(111)$ *via* Increased Surface Site Availability. *Science* **2007**, *315*, 493–497.
16. Stamenkovic, V. R.; Mun, B. S.; Arenz, M.; Mayrhofer, K. J. J.; Lucas, C. A.; Wang, G. F.; Ross, P. N.; Markovic, N. M. Trends in Electrocatalysis on Extended and Nanoscale Pt-Bimetallic Alloy Surfaces. *Nat. Mater.* **2007**, *6*, 241–247.
17. Zhang, J.; Sasaki, K.; Sutter, E.; Adzic, R. R. Stabilization of Platinum Oxygen-Reduction Electrocatalysts Using Gold Clusters. *Science* **2007**, *315*, 220–222.
18. Bauer, J. C.; Chen, X.; Liu, Q. S.; Phan, T. H.; Schaak, R. E. Converting Nanocrystalline Metals into Alloys and Intermetallic Compounds for Applications in Catalysis. *J. Mater. Chem.* **2008**, *18*, 275–282.
19. Liu, Q. S.; Yan, Z.; Henderson, N. L.; Bauer, J. C.; Goodman, D. W.; Batteas, J. D.; Schaak, R. E. Synthesis of CuPt Nanorod Catalysts with Tunable Lengths. *J. Am. Chem. Soc.* **2009**, *131*, 5720–5721.
20. Abe, H.; Matsumoto, F.; Alden, L. R.; Warren, S. C.; Abruna, H. D.; DiSalvo, F. J. Electrocatalytic Performance of Fuel Oxidation by Pt_3Ti Nanoparticles. *J. Am. Chem. Soc.* **2008**, *130*, 5452–5458.
21. Chen, W.; Kim, J. M.; Sun, S. H.; Chen, S. W. Composition Effects of FePt Alloy Nanoparticles on the Electro-oxidation of Formic Acid. *Langmuir* **2007**, *23*, 11303–11310.
22. Zhang, J.; Yang, H. Z.; Fang, J. Y.; Zou, S. Z. Synthesis and Oxygen Reduction Activity of Shape-Controlled Pt_3Ni Nanopolyhedra. *Nano Lett.* **2010**, *10*, 638–644.
23. Gasteiger, H. A.; Markovic, N.; Ross, P. N.; Cairns, E. J. Methanol Electrooxidation on Well-Characterized Pt−Ru Alloys. *J. Phys. Chem.* **1993**, *97*, 12020–12029.
24. Wang, K.; Gasteiger, H. A.; Markovic, N. M.; Ross, P. N. On the Reaction Pathway for Methanol and Carbon Monoxide Electrooxidation on Pt−Sn Alloy *versus* Pt−Ru Alloy Surfaces. *Electrochim. Acta* **1996**, *41*, 2587–2593.
25. Kang, Y. J.; Murray, C. B. Synthesis and Electrocatalytic Properties of Cubic Mn−Pt Nanocrystals (Nanocubes). *J. Am. Chem. Soc.* **2010**, *132*, 7568–7569.
26. Xu, D.; Liu, Z. P.; Yang, H. Z.; Liu, Q. S.; Zhang, J.; Fang, J. Y.; Zou, S. Z.; Sun, K. Solution-Based Evolution and Enhanced Methanol Oxidation Activity of Monodisperse Platinum−Copper Nanocubes. *Angew. Chem., Int. Ed.* **2009**, *48*, 4217–4221.
27. Greeley, J.; Stephens, I. E. L.; Bondarenko, A. S.; Johansson, T. P.; Hansen, H. A.; Jaramillo, T. F.; Rossmeisl, J.; Chorkendorff, I.; Norskov, J. K. Alloys of Platinum and Early

Transition Metals as Oxygen Reduction Electrocatalysts. *Nat. Chem.* **2009**, *1*, 552–556.
28. Kang, Y. J.; Qi, L.; Li, M.; Diaz, R. E.; Su, D.; Adzic, R. R.; Stach, E.; Li, J.; Murray, C. B. Highly Active Pt_3Pb and Core–Shell Pt_3Pb–Pt Electrocatalysts for Formic Acid Oxidation. *ACS Nano* **2012**, *6*, 2818–2825.
29. Miura, A.; Wang, H. S.; Leonard, B. M.; Abruna, H. D.; DiSalvo, F. J. Synthesis of Intermetallic PtZn Nanoparticles by Reaction of Pt Nanoparticles with Zn Vapor and Their Application as Fuel Cell Catalysts. *Chem. Mater.* **2009**, *21*, 2661–2667.
30. Ye, X.; Collins, J. E.; Kang, Y.; Chen, J.; Chen, D. T. N.; Yodh, A. G.; Murray, C. B. Morphologically Controlled Synthesis of Colloidal Upconversion Nanophosphors and Their Shape-Directed Self-Assembly. *Proc. Natl. Acad. Sci. U.S.A.* **2010**, *107*, 22430–22435.
31. Housmans, T. H. M.; Wonders, A. H.; Koper, M. T. M. Structure Sensitivity of Methanol Electrooxidation Pathways on Platinum: An On-Line Electrochemical Mass Spectrometry Study. *J. Phys. Chem. B* **2006**, *110*, 10021–10031.
32. Gregoire, J. M.; Kostylev, M.; Tague, M. E.; Mutolo, P. F.; van Dover, R. B.; DiSalvo, F. J.; Abruna, H. D. High-Throughput Evaluation of Dealloyed Pt–Zn Composition-Spread Thin Film for Methanol-Oxidation Catalysis. *J. Electrochem. Soc.* **2009**, *156*, B160–B166.
33. Yang, H.; Zhang, J.; Sun, K.; Zou, S.; Fang, J. Y. Enhancing by Weakening: Electrooxidation of Methanol on Pt_3Co and Pt Nanocubes. *Angew. Chem., Int. Ed.* **2010**, *49*, 6848–6851.